



Mechanism of compacted biochar-amended expansive clay subjected to drying–wetting cycles: simultaneous investigation of hydraulic and mechanical properties

Hao Wang^{1,2,3} · Ankit Garg^{1,2,3} · Shan Huang^{1,2,3} · Guoxiong Mei^{1,2,3}

Received: 2 January 2020 / Accepted: 28 March 2020 / Published online: 13 April 2020
© Institute of Geophysics, Polish Academy of Sciences & Polish Academy of Sciences 2020

Abstract

Biochar has been extensively studied in the aspect of amendment of compacted sandy/clayed soils, whereas its application as amendment in expansive soil is rare. Hydraulic and mechanical properties of biochar-amended expansive soil especially impacts of drying–wetting cycles have been rarely investigated. Aiming at construction of sponge city, straw biochar-amended expansive soil and the control soil (i.e., without biochar) are subjected to drying–wetting cycles in this study. During drying–wetting cycles, energy-dispersive spectrometer and Fourier transform infrared (FTIR) spectroscopy analyses were conducted to investigate microchemical composition including. Pore size distribution and microstructure were measured using nitrogen gas-adsorption technique and scanning electron microscope, respectively. Further, changes in soil water retention curve, void ratio, crack intensity factor (CIF, i.e., ratio of cracked section area to the total soil area) and shear strength were also determined. It is found that there is no difference in water retention capacity between various soils for near-saturated samples. Under high suction, however, more water could be retained within mesopores of biochar-amended soil. FTIR analysis indicates that biochar-amended expansive soil shows stronger chemical bonding, irrespective of them being subjected to drying–wetting cycles. The weak alkalinity of straw biochar results from its main chemical composition (i.e., calcium carbonate). It is noteworthy that straw biochar improves soil water retention capacity, which further restrains desiccation cracks. Cohesion of biochar–soil composite is also improved due to chemical bonding. Aiming at green roofs, straw biochar could be promising option for expansive soil amendment technically and economically.

Keywords Biochar-amended expansive soil · Sponge city · Drying–wetting cycles · Fourier transform infrared spectroscopy · Water retention

Introduction

In natural areas, rainwater could infiltrate into the ground and be returned to atmosphere via evapotranspiration. Extensive natural surfaces are covered by artificial impervious material due to large-scale urban construction. The

presence of impervious material disturbs the natural balance of infiltration and evapotranspiration (Getter and Rowe 2006). When precipitation exceeds capacity of municipal sewer system, rainwater gets mixed with raw wastewater, leading to overflowed and flood disaster. On the other hand, evapotranspiration of water from soil plays a critical role in lowering the temperature of surroundings (i.e., minimize heat island effect). Compared with natural areas, less rainwater is absorbed and then stored for evaporative cooling in cities. Based on the water absorption and storage capability of soil and plant roots, design philosophy of sponge city could mitigate urban flood disaster effectively. For instance, the green roof forms the rainwater absorbing surface, realizes the capture and temporary storage of rainwater and thus alleviates the pressure of urban drainage system.

During the construction of sponge city, projects on special soils are inevitable, and thus, relevant treatment

✉ Guoxiong Mei
meiguox@163.com

¹ College of Civil Engineering and Architecture, Guangxi University, Nanning 530004, Guangxi, China

² Key Laboratory of Disaster Prevention and Structural Safety of Ministry of Education, Guangxi University, Nanning 530004, Guangxi, China

³ Key Laboratory of Disaster Prevention and Mitigation and Engineering Safety of Guangxi, Nanning 530004, Guangxi, China

measurements should be adopted. Expansive soils are widely distributed in China, and their mechanical properties are influenced by moisture content. Compared with unsaturated expansive soil, shear strength of saturated one is much lower. Since sponge city projects are located at populous areas and exposed to natural drying–wetting cycles, more cautious consideration should be given to shear strength. On the other hand, expansive soils are unsuitable for ornamental plant because of their acidity and lack of fertility. Low saturated shear strength and lack of fertility restrict application of expansive soil in sponge city construction.

Lime and cement are commonly used as expansive soil amendments to minimize expansion and also improve their mechanical properties. However, these materials are not environment friendly for large-scale construction. One of the alternatives for improving mechanical properties of expansive soil could be biochar, which is formed by thermal decomposition of biomass (such as crop straw and livestock manure) under oxygen-deficient environment at relatively low temperature (200–700 °C) (Wong et al. 2019). The conversion of agricultural waste to biochar is a promising option for the cost reduction, control of nutrient loss and improving plant productivity (Yadav et al. 2019). It should be noted that performances of biochar on soils are influenced by feedstock of biochar. Chemical composition and structural properties are expected to be different among plant-derived biochar (PDB), manure-derived biochar (MDB) and animal-derived biochar (ADB; i.e., biochar originates from pyrolysis of animal carcasses). According to Lei et al. (2019), ADB shows high calcium (Ca; > 27%) content and relatively low carbon (C; < 8%) content, which could be used to immobilize heavy metals, instead of soil amendment for vegetation due to low carbon content. Negative effects of MDB on vegetation are also reported in previous studies (Sigua et al. 2016), and an application of poultry litter biochar leads to reduction in belowground biomass. Biochar used in this study is produced by crop straw. The conversion of straw to biochar is a promising option to mitigate the threat posed by straw combustion to the environment. Biochar is mostly alkaline, which can replace lime to modify acidity of expansive soil and provide a suitable acid–alkali environment for vegetation growth. Furthermore, biochar is highly porous and therefore provides shelter for microorganisms; they can either live in the pores or attach onto the surface of biochar (Abujabhah et al. 2018; Wong et al. 2019). In addition, porous surface assists soil to store nutrients by adsorption; thus, biochar can improve nutritional utilization of fertilizer as a sustained-release vector of fertilizer (Mukherjee and Zimmerman 2013; Chathurika et al. 2016). Biochar also takes an active part in sequestration of carbon and mitigating greenhouse effect, because CO₂ could be captured and then stored in soil by porous biochar (Ghani et al. 2013). As engineering sorbents, specific biochar can remove or immobilize

environmental contaminants, such as Pb²⁺ in polluted soil (Wang et al. 2015; Tian et al. 2019). Recent studies reveal biochar-amended clay is potential landfill final cover material to mitigate noxious gas escape to the atmosphere and minimize rainwater infiltration into the waste layer (Wong et al. 2019).

Exposed to natural conditions, green roofs are subjected to drying–wetting cycles and extreme weather inevitably. Aging of biochar is part of natural drying–wetting cycles of biochar-amended soil. According to previous studies (Mia et al. 2017; Xu et al. 2018), aged biochar contributes better to C sequestration, immobilization of heavy metal (such as Cd) and nutrient retention which further improves agricultural productivity. The effects of drying–wetting cycles on clay, especially expansive soil, have been widely studied in cracks (Tang et al. 2016), air permeability (He et al. 2017) and shear strength properties (Chowdhury and Azam 2016; Chen et al. 2018). Meeting the requirements of fertility improvement and environment protection, biochar is a promising option for expansive soil amendment. However, as potential amendment, investigation on influences of biochar on expansive soil is scarce, especially mechanical and hydraulic properties of biochar-amended expansive soil subjected to drying–wetting cycles. Without a suitable soil amendment, construction of sponge city in expansive soil areas would be restricted.

The objectives of this paper are to explore (1) effects of biochar on microstructural properties of expansive soil and (2) evolution of mechanical properties and soil water retention characteristics of biochar-amended soil under drying–wetting cycles.

Materials and methods

Test material

Two types of soil are tested in this study, i.e., bare expansive soil without biochar (named as B) and straw biochar-amended expansive soil (named as S). Based on the usage of biochar in previous studies (Reddy et al. 2015; Chen et al. 2016; Bordoloi et al. 2019; Wong et al. 2019), an amendment of 5% (w/w) is chosen as biochar application ratio. The expansive soil tested in this study was obtained from Nanning, China. Mercury intrusion porosimetry (with a 5–1,000,000 nm range; AutoPore IV 9500 mercury porosimetry, Micromeritics Instrument Corporation, USA) was conducted. The basic physical properties of tested biochar and soil are summarized in Table 1. The air-dried expansive soil and biochar were crushed and then passed through 2-mm and 0.5-mm sieves, respectively. Effects of biochar amendment in coarse textured soils are greater than in fine textured soils (Omondi et al. 2016). It is reasonably speculated that

Table 1 Basic physical properties of biochar and expansive clay tested

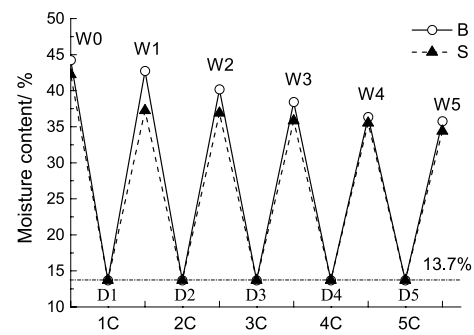
	Biochar	Expansive clay
Average pore diameter (nm)	38.3	112.3
Median pore diameter based on volume (nm)	44	121.1
Median pore diameter based on area (nm)	31.3	64.9
Liquid limit (%)	N/A	58
Plastic limit (%)	N/A	29
Liquidity index	N/A	29
Shrinkage limit (%)	N/A	16
Specific gravity	N/A	2.71
Free swelling ratio (%)	N/A	55

effects of biochar amendment for same soil increase as biochar particle size decreases (Zheng et al. 2010; Liu et al. 2016). After that, both soil and biochar were then placed in an oven at 105 °C for more than 12 h for removing any initial moisture content. For amended soil, the expansive soil and biochar were mixed proportionally (5% biochar content) and stirred after oven-drying. Both untreated and amended soils were mixed with deionized water to target moisture content of 30%. After that, slurry was sealed in a container for at least 48 h to ensure homogenization of moisture content. Soil samples were made by cutting ring with 20 mm height and 61.8 mm diameter, and the dry density of samples was controlled at $1.4 \pm 0.01 \text{ g/cm}^3$.

Drying–wetting cycles

Saturation was conducted by immersion instead of vacuum saturation, which restricted the axial swelling deformation. During saturation, swellings of samples amended with and without biochar were measured. During saturation, a vertical weight load of 2 kPa was applied on the top of each sample for simulating overburden pressure acting at very shallow depth (about 15–20 cm) in cover material (Ni et al. 2019). Such puny load is not applied by the consolidometer or any other indirect way, considering the influence of mechanical errors. The saturation time was kept more than 72 h in order to ensure degree of saturation reaching 95%. In order to control the environmental conditions of each drying process, all samples were dried using oven maintained at 105 °C. According to Liu and Sun (2017), oven-drying results in higher moisture content gradient as compared to air-drying, therefore contributing to the development of microcracks.

The simulated path of drying–wetting cycles for all samples is shown in Fig. 1. The lower limit of 13.7% is the natural air-drying moisture content, and the upper limit is saturated moisture content. Samples were first saturated to initial mass water content of W0. WnC means samples reach

**Fig. 1** Path of drying–wetting cycles

saturated moisture content for the n th time; DnC means moisture contents of samples reach 13.7% for the n th time. SnC or BnC represents biochar-amended expansive soil or control (without biochar) samples subjected to drying–wetting cycles for n th times. The value of n mentioned above could be 1, 3 and 5.

Microstructural analysis of biochar-amended expansive soil samples before and after drying wetting cycles

FTIR spectroscopy

By irradiating the sample with continuous wavelength infrared light, and recording unabsorbed infrared light, Fourier transform infrared (FTIR) spectroscopy can identify chemical compositions of the sample. Nicolet iS10 Fourier infrared spectrometer, produced by the Thermo Fisher Scientific Company, is used in this study for chemical analysis, and samples are made by KBr technique. All spectra have been treated by baseline correction, smoothing and ordinate normalization. For the spectra measured by KBr-technique, because of infrared light scattering phenomenon, there is baseline incline problem. In order to reduce influences of spectral noises and reveal the true spectral peaks covered by noises, spectral smoothing is needed. Standardized spectra obtained by ordinate normalization, in which all absorption peaks are at the range of 0 and 1, are more convenient to compare different samples.

Scanning electron microscope and energy-dispersive spectroscopy

Since different chemical elements have their own X-ray characteristics (i.e., wavelength), the element types and their amounts are measured by energy-dispersive spectroscopy. Micromorphology of sample surfaces was detected by EVO18 scanning electron microscope (SEM) equipped

with energy-dispersive spectroscopy, produced by Carl Zeiss Company.

Pore size distribution

Pore size distributions were measured by V-Sorb 4800P apparatus (GAPP Inc., China), based on nitrogen gas-adsorption technique (Jaroniec et al. 2003; Kuila and Prasad 2013). For all samples, mesopore (pore with diameter of 2–50 nm) and macropore (diameter > 50 nm) were measured, based on Barrett–Joyner–Halenda (BJH) method. And micropore (diameter < 2 nm) of biochar was measured additionally, based on Horvath–Kawazoe (HK) method. As compared to mercury intrusion porosimetry (with a range of 5–1,000,000 nm), nitrogen gas-adsorption technique (with a range of 0.35–500 nm) is more suitable for microporous biochar and biochar–soil composite.

Geotechnical testing of materials

Consolidation tests

The loading and unloading paths of consolidation tests in this study are as follows: 0 kPa → 50 kPa → 100 kPa → 200 kPa → 300 kPa → 400 kPa → 300 kPa → 200 kPa → 100 kPa → 50 kPa → 0 kPa. Each load lasted more than 24 h, until the settlement rate was lower than 0.005 mm per hour. And 72 h was required for loads of 400 kPa and 0 kPa to allow sufficient time for consolidation and re-swelling.

Direct shear tests

Strain-controlled direct shear apparatus was adopted in the test. A shear rate of 0.02 mm/min was set to limit excess pore-water pressure during shearing. Considering that the depths of biochar-amended soils are generally shallow (i.e., cover material of 0–0.3 m depth in slopes; Garg et al. 2019), the shear strength of biochar-amended soil under lower vertical load is reasonably meaningful. According to the consolidation test results, all soil samples were pre-consolidated for more than 6 h before shearing, ensuring that vertical deformations met requirements.

Soil water retention curve

In order to measure soil water retention curve, two poly (vinyl chloride) (PVC) cylindrical containers with 30 cm diameter were filled with bare soil and biochar-amended soil, respectively. The dry density of soil column was as same as cutting ring sample (i.e., 1.4 g/cm³), and the height of each saturated soil column was 20 ± 0.5 cm. One suction sensor (TEROS-21; Decagon Company) and two moisture sensors (EC-5; Decagon Company) were installed at 10 cm

soil depth of each soil column. According to previous studies (Bordoloi et al. 2019; Garg et al. 2020), gap of at least 40 mm is sufficient to prevent any interference between different sensors.

Results and discussion

Microstructural analyses

Pure biochar, B0C, B5C, S0C and S5C samples were observed at 500× and 5 K× magnifications using SEM. The images of these samples are shown in Fig. 2. There are two kinds of pores in biochar–soil composites: first, inter-pores among biochar and/or soil particles, and the second intra-pores inside biochar. As expected, biochar has higher porosity than soil samples (B0C, B5C, S0C and S5C), especially at 5 K× magnification. The observation is consistent with that of biochar obtained from water hyacinth weed and silty sand sample (Bordoloi et al. 2019). Also, B0C sample possesses larger pore size as compared to pure biochar at 500× magnification. In other words, biochar has different pore size distributions with bare soil. Intra-pore size of biochar is much lower than inter-pore size of soil, which further influences water holding capacity of soil (Gopal et al. 2019). At 500× magnification, B0C sample shows more and larger pores as compared to B5C sample. However, surface porosity of B5C sample is larger at 5 K× magnification. Biochar-amended soil also shows higher surface porosity after drying–wetting cycles at 5 K× magnification. But there is less difference between S0C and S5C samples at 500× magnification. The observations suggest that pore size distribution of both bare soil and composite is changed due to drying–wetting cycles.

In order to interpret microstructural properties after drying–wetting cycles, pore size distributions of biochar, bare soil and biochar-amended soil were further explored by nitrogen adsorption test. Since samples subjected to fewer drying–wetting cycles were still unstable, soil structure may be disturbed during preparation and testing. Therefore, only pure biochar, B5C and S5C samples were discussed. It is also of more engineering significance to study the soil structure after enough drying–wetting cycles. As shown in Fig. 3, total pore volumes of S5C and B5C are similar. However, their pore size distributions are totally different. Most pores of S5C are mesopores, because of the amendment with biochar. Only few pore diameters were larger than 50 nm (i.e., macropore) in S5C sample. For B5C sample, the macropore accounts for 40% of the total pore volume approximately.

Table 2 shows mass percentages of chemical elements for each sample obtained by energy-dispersive spectroscopy. As observed from the table, pure biochar contains around 35% carbon. Infrared absorption spectra of five samples are

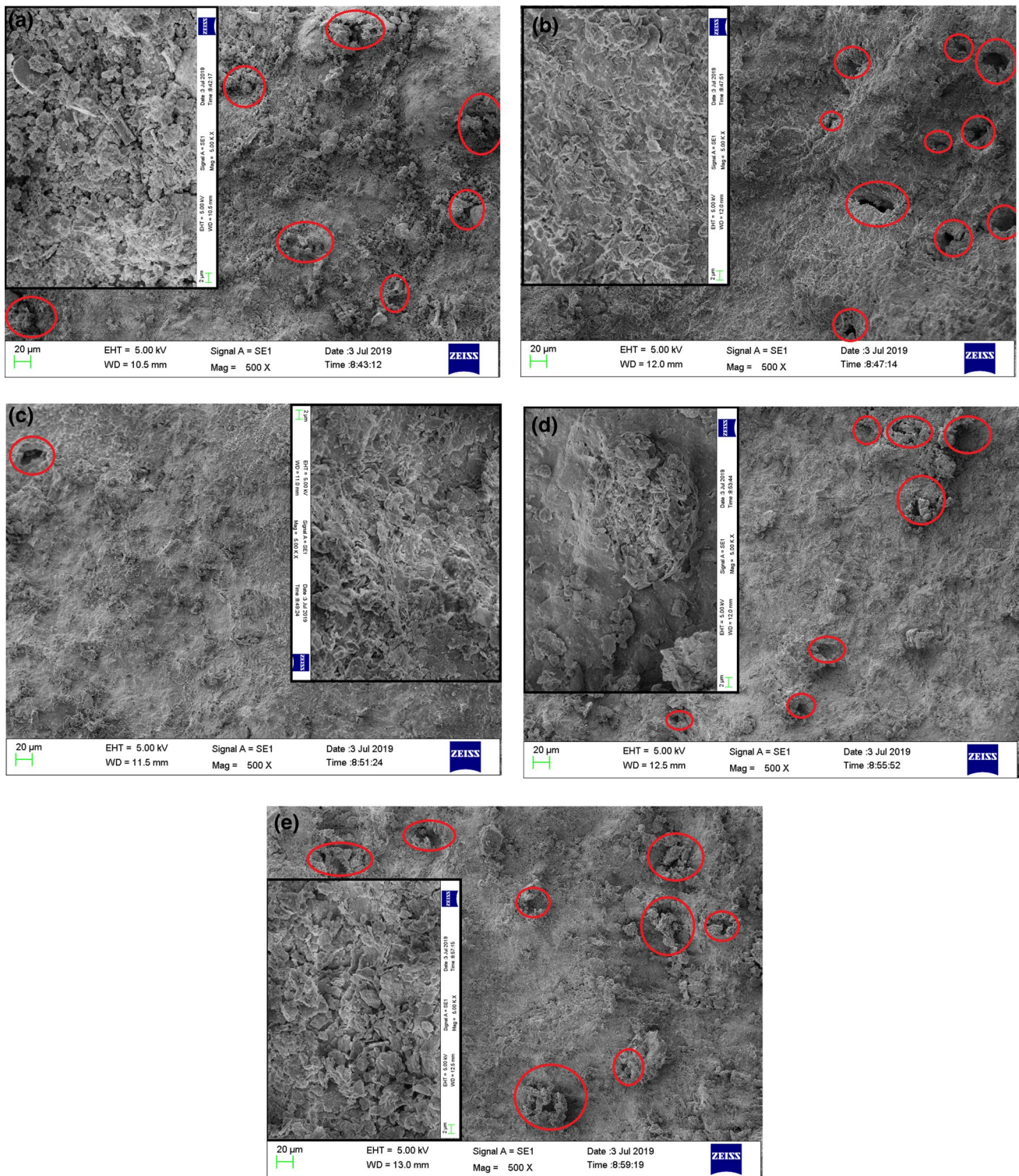


Fig. 2 SEM images of pure biochar, bare soil and biochar-amended soil before and after drying–wetting cycles **a** pure biochar, **b** B0C, **c** B5C, **d** S0C, **e** S5C

shown in Fig. 4. For each absorption peak, tangent line for lowest points at both sides of the peak was drawn as local baseline (Heller et al. 2015). The distance from the peak

point to the local baseline is taken as corrected peak height. Table 3 shows identification of absorption peaks with correction peak height greater than 0.1.

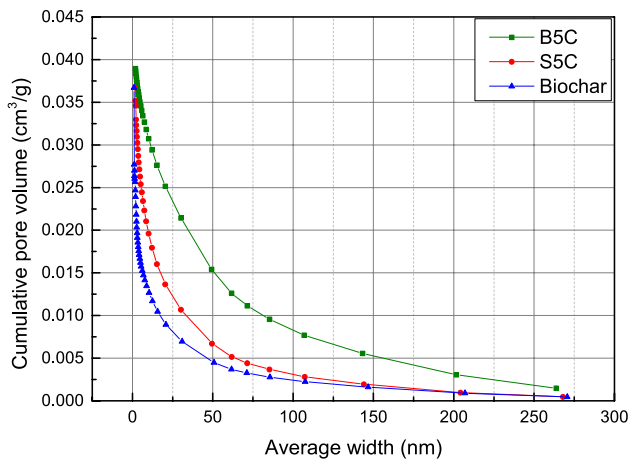


Fig. 3 Pore size distribution of biochar, bare soil and biochar-amended soil

Generally, application of biochar leads to higher soil pH as compared to unamended control soil (Chathurika et al. 2016). For biochar sample, strong absorption peaks at 1445 and 877 cm^{-1} are corresponding to carbonate bond, while bond at 604 cm^{-1} represents CaSO_4 . Neither of them is observed for all other samples. Results of energy-dispersive spectroscopy indicate that mass percentage of calcium is over 10%. Therefore, main chemical compositions of biochar are CaCO_3 and CaSO_4 . The slight alkalinity induced by CaCO_3 provides a friendly environment for most plants and bacterial communities.

For 4 soil samples, absorption peaks at 1031, 800 and 470 cm^{-1} are attributed to Si–O–Si or Si–O bond in quartz. Peak intensities in these samples follow the same order $\text{S5C} > \text{B5C} > \text{S0C} > \text{B0C}$. Interestingly, peak positions of Si–O–Si bending vibration and Fe_2O_3 are so close that their

absorption peaks coincide. These absorption peaks appear to increase with drying–wetting cycles for both biochar-amended expansive soil and the control. Biochar-amended soil shows stronger peak intensities as compared to the control irrespective of them being subjected to drying–wetting cycles. There are strong absorptions at 470 and 533 cm^{-1} resulting from Fe_2O_3 , following the same peak intensity order as Si–O bond. Illites and kaolinites are basic mineral compositions of expansive soil, which result in absorptions at 3622 and 912 cm^{-1} , respectively.

The intensity of the absorption bands depends on the amount of absorbing functional groups. This means that larger contents of functional groups are likely to result in greater intensities of the corresponding absorption bands. Iron oxide can provide cohesive force partly by cementing soil particles. Cohesion resulting from chemical bonds is determined by bond strength or so-called bond energy. With 452 kJ mol^{-1} bond energy, Si–O bond is a kind of strong chemical bond. FTIR results indicate that biochar-amended soil possesses more cementations and chemical bonds to provide cohesion as compared to bare expansive soil.

Consolidation of biochar-amended expansive soil

Swelling ratios of saturated samples subjected to different drying–wetting cycles are shown in Fig. 5. With an increase in drying–wetting cycles, the irreversible compaction of expansive soil occurs. Comparatively smaller biochar particles are embedded into relatively larger pores of soil particles, leading to a higher degree of compaction (Chowdhury and Azam 2016), and thus lower void ratio. Before drying–wetting cycles, saturated swelling of S0C sample is slightly larger than that of B0C sample. Beyond that, the biochar mitigates the swelling characteristic of expansive soil

Table 2 Mass percentages of chemical elements

Element	Atomic number	Biochar/%	B0C/%	B5C/%	S0C/%	S5C/%
Carbon	6	34.57	26.22	22.8	27.4	26.38
Oxygen	8	17.78	32.25	26.85	24.5	33.68
Sodium	11		0.06	0	0	0
Magnesium	12	1.11	0.43	0.25	0.01	0.03
Aluminum	13	4.4	9.82	10.46	12.94	14.25
Silicon	14	5.62	11.34	13.57	10.37	16.44
Phosphorus	15	0.76				
Sulfur	16	1.51				
Chlorine	17	1.69				
Potassium	19	3.75	1.75	1.07	0.86	0.81
Calcium	20	10.27		0.11	0.31	0.19
Titanium	22		0.35	0.22	0.13	0.18
Iron	26	0.76	1.52	2.12	1.69	2.51
Zirconium	40		2.45			
Total		82.22	86.19	77.45	78.21	94.47

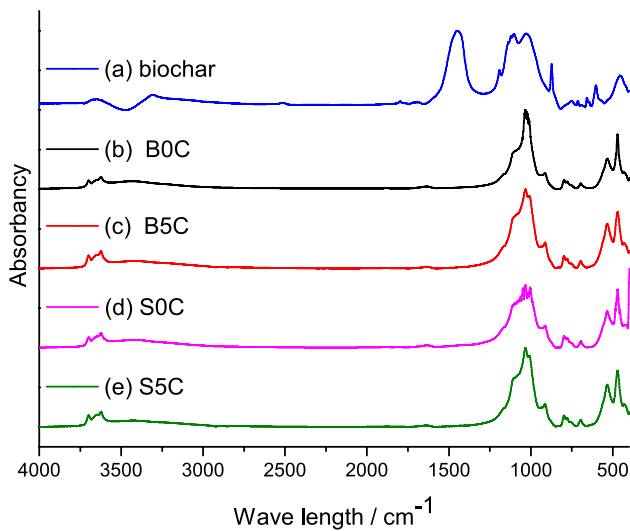


Fig. 4 FTIR spectra of biochar and soils before and after drying–wetting cycles

effectively (Zong et al. 2014). The swelling of S5C sample is significantly lower than that of B5C after repeated shrinkages and swellings. With repeated drying and wetting, swelling properties of both B and S samples weaken and then tend to be stable. At the first drying–wetting cycle, the height of S sample decreases from 24.0 mm to 22.2 mm (i.e., swelling ratio decreases from 20% to 11%) dramatically, while that of B sample decreases gradually during 5 cycles.

The dry density of all soil samples is 1.4 g/cm^3 ; the specific gravity of bare and biochar-amended soils is 2.71 and 2.69, respectively. Therefore, the void ratio could be calculated after measuring sample heights using vernier caliper and dial gage. Void ratios of S samples and B samples under same drying–wetting cycles are compared (refer to Fig. 6). Before drying–wetting cycles, void ratios of two soil samples are similar. Under low pressure, void ratio of S0C sample is smaller than that of B0C sample, while the opposite is true under high pressure. The compaction effect of drying–wetting cycles on biochar-amended soil is more crucial. After the first drying–wetting cycle, void ratio of S sample under different vertical loads is lower than that of B sample.

Void ratios of B samples and S samples under different stages of drying–wetting cycles are shown in Fig. 7a, b, respectively. Before vertical loads are applied, initial void ratios of two kind of saturated soil samples decrease with cyclic drying and wetting. The results are similar to those obtained by previous studies (Kholghifard et al. 2014; Chen et al. 2018) for only bare soil (i.e., without biochar). Both bare and amended soil samples are influenced by compaction effect induced by drying–wetting cycles. However, the effect on biochar-amended soil is more prominent. The decrease from S0C to S1C is larger than that from S1C to S5C, indicating that more micro-disintegrations of soil have likely occurred during the first cycle as compared to the subsequent cycles.

Table 3 Functional group identification

Peak position/ cm-1	Corrected peak height					Assignment	Representative characterization	References
	Pure biochar	B0C	B5C	S0C	S5C			
3622	0.025	0.078	0.069	0.056	0.104	O–H stretching of phyllosilicates, Fe and Al oxides	Illite	Xiao et al. (2018)
3309	0.177	NF	NF	NF	NF	Intermolecular hydrogen bonds		Gu et al. (2016)
1445	0.851	NF	NF	NF	NF	Antisymmetric stretching vibration of CO_3^{2-}	Carbonate	Du (2012), Frost et al. (2015), Linker et al. (2005)
1031	0.255	0.093	0.123	0.103	0.153	Stretching of Si–O	Quartz	Linker et al. (2005), Wu et al. (2014), Heller et al. (2015), Liang et al. (2018)
912	NF	0.083	0.147	0.081	0.164	–OH	Kaolinite	Du (2012), Wu et al. (2014)
877	0.386	NF	NF	NF	NF	CO_3^{2-}	Carbonate	Du (2012), Frost et al. (2015), Reig et al. (2002)
800	NF	0.052	0.083	0.067	0.128	Si–O–Si	Quartz	Reig et al. (2002)
604	0.223	NF	NF	NF	NF	CaSO_4		Choe et al. (2010)
533	NF	0.201	0.303	0.222	0.496	Fe_2O_3	Hematite	Weng and Xu (2016), Schwertmann and Cornell (2000)
470	NF	0.266	0.38	0.342	0.41	Bending vibration of Si–O–Si Fe_2O_3	Quartz Hematite	Reig et al. (2002), Wu (1994) Schwertmann et al. (1998), Schwertmann and Cornell (2000)

NF not found

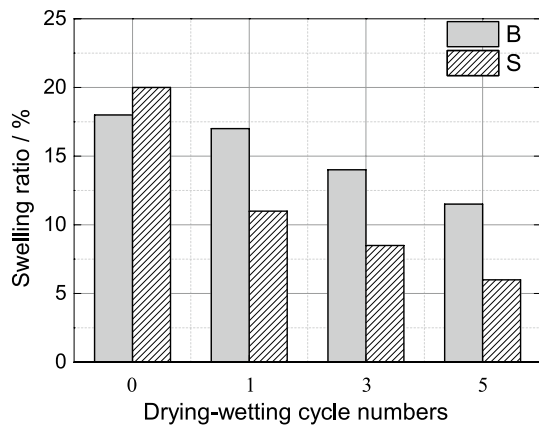


Fig. 5 Swelling ratio of saturated samples under drying-wetting cycles

Water retention and crack development

Soil–water retention curves (i.e., the relationship of volumetric water content (VWC) and matric suction) are shown in Fig. 8. Under low suction (less than 100 kPa, i.e., near-saturated moisture content), water retention capacities of B and S samples are approximately similar. However, more water could be held in S samples under high suction (especially when suction exceeds 1000 kPa). In other words, water retention capacity of unsaturated expansive clay is improved

by biochar. Considering pore size distribution of soil–biochar composite, this phenomenon could be explained. For near-saturated soil samples, suction mainly influences water within macropores. With decreasing moisture content, more suction is needed to extract water from mesopores as compared to macropores. Mesopores (as shown in Fig. 3) created by biochar in soil–biochar composite contribute to water retention capacity via capillarity.

Further, it is possible that biochar could inhibit crack propagation due to improved soil–water retention capacity. According to Zhang (Zhang et al. 2020), cracking behaviors are affected by biochar mainly in evaporation process. Crack intensity factor (CIF, i.e., ratio of cracked section area to the total soil area) is used to show crack development quantitatively in this study. As shown in Fig. 9a, crack images were inputted to ImageJ software and converted to grayscale images. After the thresholding and de-noising, final images were obtained where it was easy to calculate pixel numbers of cracked and intact parts of soil. For each sample, average CIF was calculated by 4 parallel samples, as shown in Fig. 9b. Desiccation cracks would emanate from the surface when tensile force induced by air–water menisci surpasses soil strength (Li et al. 2009). After the first cycle, main cracks are formed in B samples. Widths of main cracks tend to increase along with development of secondary cracks gradually during subsequent drying–wetting cycles. After the fourth cycle, subsequent cycles have

Fig. 6 Variation of void ratio with different soil samples **a** 0C samples, **b** 1C samples, **c** 3C samples, **d** 5C samples

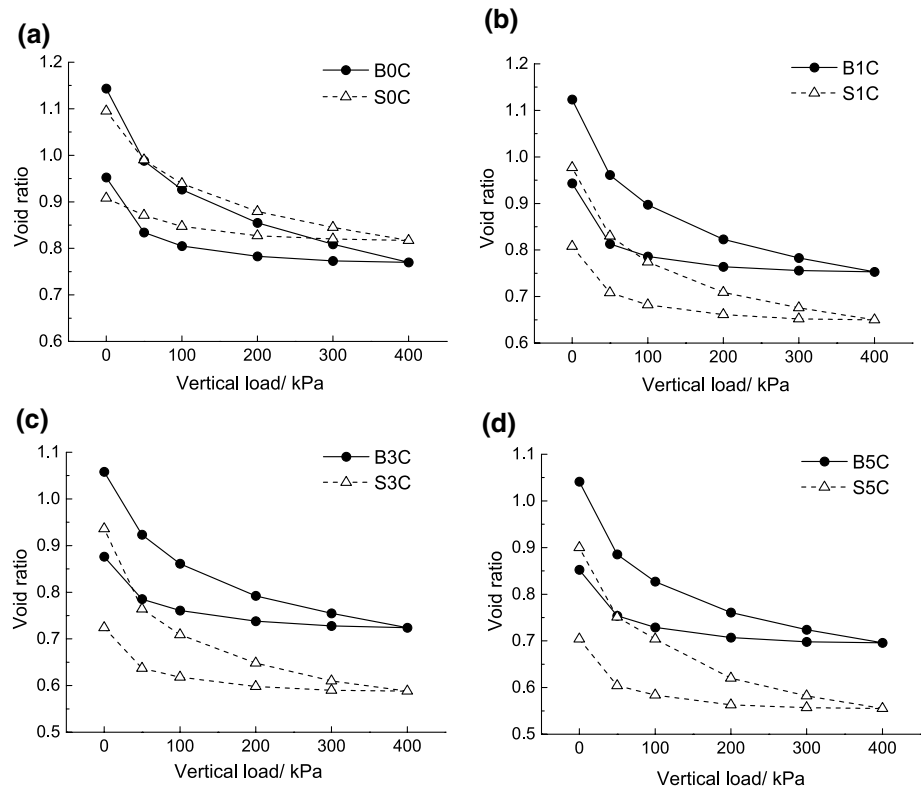


Fig. 7 Variation of void ratio with cycle numbers **a** B samples, **b** S samples

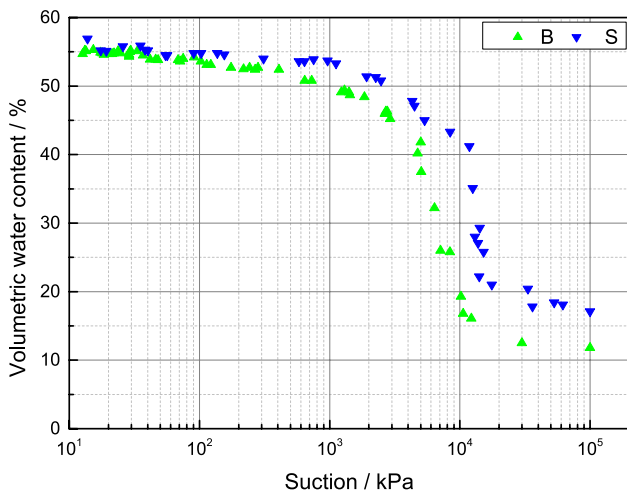
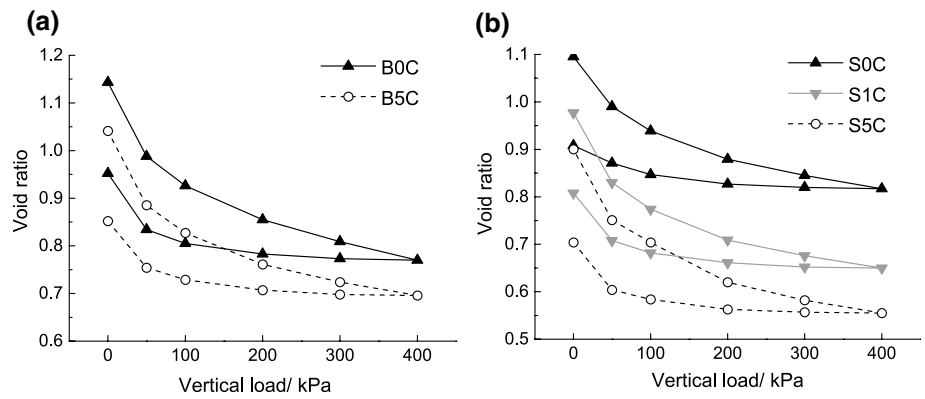


Fig. 8 Soil water retention curves of bare soil and biochar-amended soil

negligible influence on further crack development, and CIF tends to be stable. The crack development of S samples lags behind that of B samples. There is only shrinkage deformation without any macroscopic crack during the first cycle; therefore, CIF value is close to zero. However, shrinkage further results in breaking of microbonding and rearrangement of soil structure. This implies that soil strength has been actually reduced during shrinkage. Thus, soil sample may do not possess enough strength to resist surface tensile force in the following cycle. Crack intensity factor decreases due to the presence of biochar (Zong et al. 2014; Bordoloi et al. 2019; Zhang et al. 2020). Main cracks of S samples appear at the second cycle, but CIF is still less than that of B samples. This phenomenon can be explained as followed: On the one hand, straw biochar improves soil–water retention capacity (as shown in Fig. 8), as reported for other porous biochar (Wong et al. 2019). There are two kinds of pores

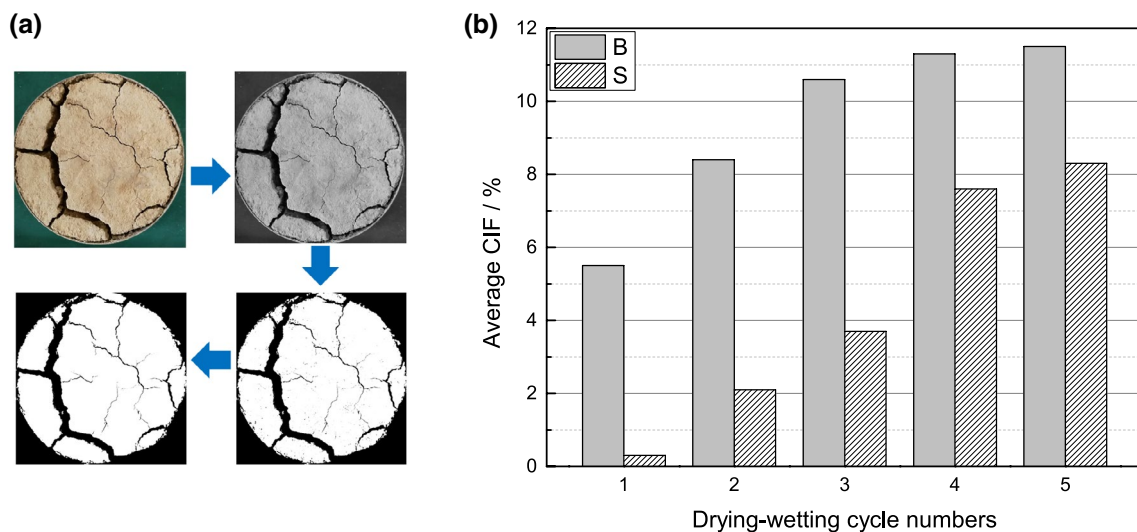


Fig. 9 Measurement and comparison of crack intensity factor (CIF) **a** procedures of measuring CIF, **b** CIF of bare soil and biochar–soil composite under drying–wetting cycles

in biochar–soil composite: first, inter-pores among biochar and/or soil particles, and the second intra-pores inside biochar (refer to Fig. 2). As compared to bare soil, intra-pores of biochar make the composite susceptible to absorb and hold additional water (Lu et al. 2014; Bordoloi et al. 2019). For bare soil, water within macropores is relatively easy to be extracted under evaporation. For biochar-amended soil, however, water held in mesopores and micropores (mainly in biochar) helps to resist crack propagation. On the other hand, biochar particles filled in soil particles generate the Fe_2O_3 cement according to the FTIR analysis results (refer to Fig. 4). Such cement bonds soil particles in weak area, thus delaying the generation of cracks.

Shear strength

The low shear strength of saturated expansive soil limits its application in the field of sponge city. In order to compare saturated shear strength, the cohesive force and angle of internal friction of two kinds of soils are shown in Fig. 10a, b, respectively. In general, both angles of internal friction and cohesive force of S samples are higher than those of B samples. This indicates that the shear strength of saturated expansive soil is improved by addition of biochar. According to Lu et al. (2014), rice husk biochar improves internal friction angle of expansive clay before drying–wetting cycles. With an increase in cycle numbers, transition from decrease to increase is observed for cohesive force of both S and B samples, but at different inflection points. For B samples, cohesive force decreases sharply during the first cycle and then rises gradually and eventually stabilizes. For S samples, cohesive force decreases to the minimum at the third cycle, but the minimum value is much greater than that of B samples. After 5 drying–wetting cycles, cohesive force of B samples is slightly lower than that of the original state, while S samples show stronger cohesion compared with the original state. FTIR analysis (refer to Fig. 4) shows that biochar-amended soil is more susceptible to microchemical changes induced by drying–wetting cycles. More cementation and chemical bonds provide stronger cohesive force for

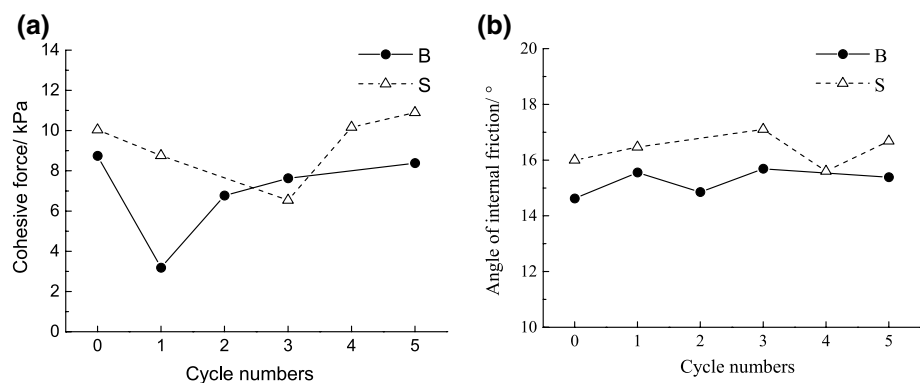
S5C sample as compared to B5C sample. For both B and S samples, angle of internal friction fluctuates within a certain range, which is similar to previous test results for bare soil (Dong et al. 2019; Huang et al. 2019). After the fifth cycle, subsequent cycles have little influence on cohesive force (Dong et al. 2019; Huang et al. 2019).

There are mainly 3 factors by which drying–wetting cycles affect shear strength: (1) crack development; (2) increasing chemical bonds and cementation; (3) reducing void ratio. Development of crack damages shear strength of soil samples, while the latter two factors are beneficial to the improvement of shear strength.

The presence of cracks would form weak zones and significantly damage soil structure, thus causing reduction in the overall mechanical strength (Tang et al. 2012; He et al. 2017; Chen et al. 2018; Huang et al. 2019). At the same cycle number, there are more and wider cracks (i.e., higher CIF) in B samples as compared to S samples. During the first cycle, main cracks are formed in B samples, which destroy the original structure of soil samples and create weak zones, so cohesive force reaches the minimum value. However, for S samples only shrinkage deformation and small cracks occur during the first two cycles, and cohesive force decreases gradually. At the third cycle, main cracks emanate, and cohesive force of S sample reaches the minimum value.

After crack propagation reaches a certain scale, increasing microchemical bonding and decrease in void ratio play dominant roles in affecting shear strength. The cementation and chemical bonds between soil particles contribute to cohesion partly. FTIR results indicate that drying–wetting cycles improve shear strength by forming more cements and chemical bonds, such as Fe_2O_3 and Si–O bond. Drying–wetting cycles not only produce damages but also densify soil samples (Chen et al. 2018). Void ratios of both B and S samples decrease after repeated drying–wetting cycles. According to previous studies (Zhang and Wang 2018; Dong et al. 2019), the peak and steady-state shear strengths increase as void ratio decreases. Biochar-amended soil is more susceptible to the compaction effect, after 5 drying–wetting cycles biochar-amended soil is relatively denser than the control.

Fig. 10 Shear strength of bare soil and biochar-amended soil under drying–wetting cycles **a** cohesive force, **b** angle of internal friction



Feasibility and cost–benefit analysis

As far as the authors are aware, green roof substrate could be designed as multilayers. Compacted biochar-amended clays could be used as multifunctional layer below the vegetated soil layer. On the one hand, roots could relatively easily develop and elongate in loose soil. Compacted biochar-amended clays may act as root-barrier layer, due to its inhibition to root expansion and elongation. On the other hand, soil water retention is much more critical in green roofs as compared to agricultural fields. It is more feasible and reasonable to store rainwater in soil as compared to frequent irrigation. More rainwater could be stored in biochar-amended clay due to improved soil–water retention capacity (refer to Fig. 8).

Biochar-amended clays could contribute well to reduction in maintenance cost of green roofs. On the one hand, irrigation costs may be noticeable in green roofs, considering no groundwater could be utilized. Frequent irrigation could be avoided as results of improved soil water retention capacity. On the other hand, ornamental plants are generally expensive and highly environmentally demanding. More water and nutrient could be provided by biochar-amended soil, further ensuring flourishing of ornamental plants. Potential economic losses could be avoided via amendment with biochar. The cost of biochar amendment could be easily covered by economic benefits mentioned above.

Conclusions

As far as the authors are aware, investigation on influences of biochar on compacted expansive clay is scarce, especially taking drying–wetting cycles into consideration. The study aims to explore mechanism of hydraulic and mechanical behaviors of biochar-amended expansive clay subjected to drying–wetting cycles. The following conclusions can be drawn:

- (1) Infrared spectrum indicates that the weak alkalinity of straw biochar results from its main chemical composition, calcium carbonate. Chemical bonds and cementation between soil particles contribute to cohesive force partly. Drying–wetting cycles enhance these chemical bonding effects, especially for biochar-amended soil.
- (2) Under high suction, biochar–soil composite shows greater water retention capacity as compared to bare soil due to pore size distribution. There are more mesopores in biochar-amended soil instead of macropores. Water held in mesopores is relatively hard to be extracted under evaporation, which further influences crack propagation. For near-saturated soil samples, suction mainly influences water within macropores. There-

fore, the difference between water retention capacities of bare and biochar-amended soils is negligible under low suction.

- (3) For both bare expansive clay and biochar-amended soil, drying–wetting cycles can reduce void ratio and restrain swelling behavior. Biochar-amended soil is more susceptible to compaction effect induced by drying–wetting cycles. Biochar can restrain the formation and propagation of soil cracks. In general, both angles of internal friction and cohesive force of expansive soil are improved by the addition of biochar. Drying–wetting cycles are likely to influence shear strength mainly through formation of microchemical bonding, reducing void ratio and CIF.
- (4) Aiming at green roofs, biochar has potential values to act as amendment in soil substrate economically and technically. Frequent irrigation could be avoided by amendment with biochar due to improved soil water retention capacity.

Acknowledgements The authors would like to acknowledge the State Key Laboratory for the protection and utilization of subtropical agricultural biological resources at Guangxi University for providing the setup for the FTIR analysis. And the authors would like to express their sincere gratitude to National Natural Science Foundation of China (Grant Nos. 51578164 and 51878185) and Innovative Research Team Program of Guangxi Natural Science Foundation (Grant No. 2016GXNSFGA380008) for support.

Compliance with ethical standards

Conflict of interest All authors declare that there is no conflict of interest.

References

- Abujabbar IS, Doyle RB, Bound SA, Bowman JP (2018) Assessment of bacterial community composition, methanotrophic and nitrogen-cycling bacteria in three soils with different biochar application rates. *J Soils Sediments* 18:148–158
- Bordoloi S, Gopal P, Boddu R, Wang Q, Cheng YF, Garg A, Sreedeeep S (2019) Soil-biochar-water interactions: role of biochar from *Eichhornia crassipes* in influencing crack propagation and suction in unsaturated soils. *J Clean Prod* 210:847–859
- Chaturika JAS, Kumaragamage D, Zvomuya F, Akinremi OO, Flaten DN, Indraratne SP, Dandeniya WS (2016) Woodchip biochar with or without synthetic fertilizers affects soil properties and available phosphorus in two alkaline, chernozemic soils. *Can J Soil Sci* 96:472–484
- Chen XW, Wong JTF, Ng CWW, Wong MH (2016) Feasibility of biochar application on a landfill final cover—a review on balancing ecology and shallow slope stability. *Environ Sci Pollut Res* 23:7111–7125
- Chen R, Xu T, Lei W, Zhao Y, Qiao J (2018) Impact of multiple drying–wetting cycles on shear behaviour of an unsaturated compacted clay. *Environ Earth Sci* 77:683–691

- Choe E, van der Meer F, Rossiter D, van der Salm C, Kim KW (2010) An alternate method for Fourier Transform Infrared (FTIR) spectroscopic determination of soil nitrate using derivative analysis and sample treatments. *Water Air Soil Pollut* 206:129–137
- Chowdhury RH, Azam S (2016) Unsaturated shear strength properties of a compacted expansive soil from Regina, Canada. *Innov Infrastruct Solut* 1:47–57
- Dong JG, Xu GY, Lv HB, Yang JY (2019) Prediction of expansive soil strength based on micro-scale properties. *Geotech Geol Eng* 37:869–882
- Du CW (2012) Principle and application of soil infrared photoacoustic spectroscopy. Science Press, Beijing (**in Chinese**)
- Frost RL, Scholz R, Lopez A (2015) Infrared and Raman spectroscopic characterization of the carbonate bearing silicate mineral aerinite - implications for the molecular structure. *J Mol Struct* 1097:1–5
- Garg A, Hazra B, Zhu H, Wen Y (2019) A simplified probabilistic analysis of water content and wilting in soil vegetated with non-crop species. *CATENA* 175:123–131
- Garg A, Huang H, Kushvaha V, Madhushri P, Kamchoom V et al (2020) Mechanism of biochar soil pore–gas–water interaction: gas properties of biochar-amended sandy soil at different degrees of compaction using KNN modeling. *Acta Geophys* 68:207–217
- Getter KL, Rowe DB (2006) The role of extensive green roofs in sustainable development. *HortScience* 41:1276–1285
- Ghani WAWAK, Mohd A, Da Silva G, Bachmann RT, Taufiq-Yap YH et al (2013) Biochar production from waste rubber-wood-sawdust and its potential use in C sequestration: chemical and physical characterization. *Ind Crops Prod* 44:18–24
- Gopal P, Bordoloi S, Ratnam R et al (2019) Investigation of infiltration rate for soil–biochar composites of water hyacinth. *Acta Geophys* 67:231–246
- Gu J, Hao L, Huang PF, Tong N, Li X, Yin GH (2016) FTIR and ESEM analysis of soil moisture microscopic conservation feature with liquid membrane. In: The international seminar on applied physics, optoelectronics and photonics. <https://doi.org/10.1051/mateconf/20166101022>
- He Y, Cui YJ, Ye WM, Conil N (2017) Effects of wetting-drying cycles on the air permeability of compacted Teguline clay. *Eng Geol* 228:173–179
- Heller C, Ellerbrock RH, Roskopf N, Klingenfuss C, Zeitz J (2015) Soil organic matter characterization of temperate peatland soil with FTIR-spectroscopy: effects of mire type and drainage intensity. *Eur J Soil Sci* 66:847–858
- Huang Z, Wei B, Zhang L, Chen W, Peng Z (2019) Surface crack development rules and shear strength of compacted expansive soil due to dry-wet cycles. *Geotech Geol Eng* 37:2647–2657
- Jaroniec M, Choma J, Kruk M (2003) Assessment of reliability of the Horvath–Kawazoe pore size analysis method using argon adsorption isotherms on ordered mesoporous silicas. *Colloids Surf A* 214:263–269
- Kholghifard M, Ahmad K, Ali N, Kassim A, Kalatehjari R (2014) Collapse/swell potential of residual laterite soil due to wetting and drying–wetting cycles. *Natl Acad Sci Lett* 37:147–153
- Kuila U, Prasad M (2013) Specific surface area and pore-size distribution in clays and shales. *Geophys Prospect* 61(2):341–362
- Lei SC, Shi Y, Qiu YP, Che L, Xue C (2019) Performance and mechanisms of emerging animal-derived biochars for immobilization of heavy metals. *Sci Total Environ* 646:1281–1289
- Li JH, Zhang LM, Wang Y, Fredlund DG (2009) Permeability tensor and representative elementary volume of saturated cracked soil. *Can Geotech J* 46:928–942
- Liang D, Du CW, Ma F, Shen YZ, Wu K, Zhou JM (2018) Degradation of Polyacrylate in the outdoor agricultural soil measured by FTIR-PAS and LIBS. *Polymers* 10(12):1296–1304
- Linker R, Shmulevich I, Kenny A, Shaviv A (2005) Soil identification and chemometrics for direct determination of nitrate in soils using FTIR-ATR mid-infrared spectroscopy. *Chemosphere* 61(5):652–658
- Liu W, Sun X (2017) Comparison of two drying/wetting methods for assessing the influence of drying/wetting on the mechanical cyclic behaviors of soils. *Iran J Sci Technol Trans Civ Eng* 41:297–303
- Liu ZL, Dugan B, Masiello CA, Barnes RT, Gallagher ME, Gonnermann H (2016) Impacts of biochar concentration and particle size on hydraulic conductivity and DOC leaching of biochar–sand mixtures. *J Hydrol* 533:461–472
- Lu SG, Sun FF, Zong YT (2014) Effect of rice husk biochar and coal fly ash on some physical properties of expansive clayey soil (Vertisol). *CATENA* 114:37–44
- Mia S, Dijkstra FA, Singh B (2017) Chapter one—long-term aging of biochar: a molecular understanding with agricultural and environmental implications. *Adv Agron* 141:1–51
- Mukherjee A, Zimmerman AR (2013) Organic carbon and nutrient release from a range of laboratory-produced biochars and biochar-soil mixtures. *Geoderma* 193:122–130
- Ni J, Bordoloi S, Ankit G, Wei S, Sreedeeep S (2019) Simple model on water retention and permeability in soil mixed with lignocellulose fibres. *KSCE J Civ Eng* 23:138–146
- Omondi MO, Xia X, Nahayo A, Liu XY, Korai PK, Pan GX (2016) Quantification of biochar effects on soil hydrological properties using meta-analysis of literature data. *Geoderma* 274:28–34
- Reddy KR, Yaghoubi P, Yukselen-Aksoy Y (2015) Effects of biochar amendment on geotechnical properties of landfill cover soil. *Waste Manag Res* 33:524–532
- Reig FB, Adelantado JVG, Moreno MCMM (2002) FTIR quantitative analysis of calcium carbonate (calcite) and silica (quartz) mixtures using the constant ratio method. Application to geological samples. *Talanta* 58:811–821
- Schwertmann U, Cornell RM (2000) Iron oxides in the laboratory. Wiley, New York
- Schwertmann U, Friedl J, Stanjek H, Murad E, Koch CB (1998) Iron oxides and smectites in sediments from the Atlantis II Deep, Red Sea. *Eur J Miner* 10:953–967
- Sigua GC, Novak JM, Watts DW, Johnson MG, Spokas K (2016) Efficacies of designer biochars in improving biomass and nutrient uptake of winter wheat grown in a hard setting subsoil layer. *Chemosphere* 142:176–183
- Tang CS, Shi B, Cui YJ, Liu C, Gu K (2012) Desiccation cracking behavior of polypropylene fiber-reinforced clayey soil. *Can Geotech J* 49:1088–1101
- Tang CS, Wang DY, Shi B, Li J (2016) Effect of wetting-drying cycles on profile mechanical behavior of soils with different initial conditions. *CATENA* 139:105–116
- Tian R, Li CX, Xie SY et al (2019) Preparation of biochar via pyrolysis at laboratory and pilot scales to remove antibiotics and immobilize heavy metals in livestock feces. *J Soils Sediments* 19:2891–2902
- Wang ZY, Liu GC, Zheng H et al (2015) Investigating the mechanisms of biochar's removal of lead from solution. *Bioresour Technol* 177:308–317
- Weng SF, Xu YZ (2016) Fourier transform infrared spectrum analysis. Chemical Industry Press, Beijing (**in Chinese**)
- Wong JTF, Chen X, Deng W, Chai Y, Ng CWW, Wong MH (2019) Effects of biochar on bacterial communities in a newly established landfill cover topsoil. *J Environ Manag* 236:667–673
- Wu JG (1994) Modern Fourier transform infrared spectroscopy and its application. Science and Technology Literature Press, Beijing (**in Chinese**)
- Wu HY, Chen WL, Rong XM, Cai P, Dai K, Huang QY (2014) In situ ATR-FTIR study on the adhesion of *Pseudomonas putida* to Red soil colloids. *J Soil Sediment* 14(3):504–514
- Xiao J, Wen YL, Yu GH, Dou S (2018) Strategy for microscale characterization of soil mineral-organic associations by

- synchrotron-radiation-based FTIR technology. *Soil Sci Soc Am J* 82(6):1583–1591
- Xu ZB, Xu XY, Tsang DCW, Cao XD (2018) Contrasting impacts of pre- and post-application aging of biochar on the immobilization of Cd in contaminated soils. *Environ Pollut* 242:1362–1370
- Yadav V, Karak T, Singh S, Singh AK, Khare P (2019) Benefits of biochar over other organic amendments: responses for plant productivity (*Pelargonium graveolens* L.) and nitrogen and phosphorus losses. *Ind Crops Prod* 131:96–105
- Zhang F, Wang G (2018) Effect of irrigation-induced densification on the post-failure behavior of loess flowslides occurring on the Heifangtai area, Gansu, China. *Eng Geol* 236:111–118
- Zhang YP, Gu K, Li JW, Tang CS, Shen ZT, Shi B (2020) Effect of biochar on desiccation cracking characteristics of clayey soils. *Geoderma*. <https://doi.org/10.1016/j.geoderma.2020.114182>
- Zheng W, Guo MX, Chow T, Bennett DN, Rajagopalan N (2010) Sorption properties of greenwaste biochar for two triazine pesticides. *J Hazard Mater* 181:121–126
- Zong Y, Chen D, Lu S (2014) Impact of biochars on swell-shrinkage behavior, mechanical strength, and surface cracking of clayey soil. *J Plant Nutr Soil Sci* 177:920–926